Torque Production Limit of Surface Permanent Magnet Synchronous Machines and their Electromagnetic Scalability

Ge, Baoyun; Liua, Mingda; Dong, Jianning; Liu, Wenbo

DOI
10.1109/TIA.2021.3084552

Publication date
2021

Document Version
Final published version

Published in
IEEE Transactions on Industry Applications

Torque Production Limit of Surface Permanent Magnet Synchronous Machines and Their Electromagnetic Scalability

Baoyun Ge, *Member, IEEE*, Mingda Liu, *Member, IEEE*, Jianning Dong, and Wenbo Liu, *Member, IEEE*

***Abstract*—In view of the increasing demand in torque density, this article propounds the idea of looking for an upper bound of the torque production and average shear stress for surface permanent magnet (SPM) synchronous machines. The derivation is based on the assumption of an infinite permeability of the iron core and employs the transfer relation between the normal magnetic flux density and the tangential magnetic strength. The result is written as functions of the machine's major geometries and excitation conditions. The ratio of the actual value and this upper bound may be used as a metric of measuring the usage of materials' electromagnetic capability, or reversely as an indicator of the marginal gain of the iron core of higher relative permeability. The result is further investigated to discuss the electromagnetic scalability and the sizing law of SPM machines. Specifically, the reason for increasing volumetric torque density as the machine size goes up is revealed. The optimal remanence flux density of permanent magnets is also predicted at 1.91 T, providing that the lamination saturates at 2 T.**

***Index Terms*—Scalability, shear stress, surface permanent magnet (SPM), torque density.**

NOMENCLATURE

$\mathbf{B}$	Magnetic flux density $[\mathrm{T}]$.
$\mathbf{H}$	Magnetic field strength $[\mathrm{A/m}]$.
$\mathbf{M}$	Magnetization vector of PMs $[\mathrm{A/m}]$.
B_{sat}	Iron saturation level $[\mathrm{T}]$.
B_r	Remanence flux density $[\mathrm{T}]$.
C_s	Number of parallel circuits $[-]$.
I_{sp}	Stator peak current $[\mathrm{A}]$.
$\widetilde{K}$	Current loading or linear current density $[\mathrm{A/m}]$.
$\widetilde{M_r}$	Magnetization in the r-direction $[\mathrm{A/m}]$.
N_t	Stator winding total number of turns $[-]$.
P	Pole pairs $[-]$.
T_e	Electromagnetic torque $[\mathrm{N\cdot m}]$.
$\mathrm{V}_s, \mathrm{V}_r$	Stator and rotor volumes, respectively $[\mathrm{m}^3]$.
f_m, g_m	Geometric functions $[-]$.
g	Air-gap length $[\mathrm{m}]$.
h	Harmonic order $[-]$.
$k_{s,h}, k_{r,h}$	Stator and rotor winding factors, respectively $[-]$.
l_e	Effective axial length $[\mathrm{m}]$.
$r_m, r_{\mathrm{or}}, r_{\mathrm{is}}$	Radius of various surfaces $[\mathrm{m}]$.
α_m	Magnets pole–arc to pole–pitch ratio $[-]$.
$\theta, \theta_e, \theta_r$	Mechanical, electrical, and rotor angles, respectively $[\mathrm{rad}]$.
μ_0	Vacuum permeability $[\mathrm{H/m}]$.
μ_{rm}	Relative permeability of PMs $[-]$.
$\bar{\sigma}_m$	Average shear stress $[\mathrm{Pa}]$ or $[\mathrm{psi}]$.
$\widetilde{\varphi}$	Magnetic scalar potential $[\mathrm{A}]$.
ω_e	Synchronous angular speed $[\mathrm{rad/s}]$.

Manuscript received April 27, 2020; revised July 28, 2020, October 23, 2020, and March 5, 2021; accepted May 1, 2021. Date of publication May 27, 2021; date of current version September 16, 2021. Paper 2020-EMC-0774, presented at the 2019 Energy Conversion Congress & Exposition, Baltimore, MD, USA, Sep. 29–Oct. 3, and approved for publication in the IEEE TRANSACTIONS ON INDUSTRY APPLICATIONS by the Electric Machines Committee of the IEEE Industry Applications Society. *(Corresponding author: Baoyun Ge.)*

Baoyun Ge is with the C-Motive Technologies, Inc., Madison, WI 53704 USA (e-mail: baoyun@c-motive.com).

Mingda Liu is with the Carpenter Technology Corporation, Philadelphia, PA 19601 USA (e-mail: mliu239@wisc.edu).

Jianning Dong is with the Department of Electrical Sustainable Energy, Delft University of Technology, 2628 Delft, The Netherlands (e-mail: J.Dong-4@tudelft.nl).

Wenbo Liu is with the Ford Motor Company, Deerborn, MI 48124 USA (e-mail: wliu89@ford.com).

Color versions of one or more figures in this article are available at https://doi.org/10.1109/TIA.2021.3084552.

Digital Object Identifier 10.1109/TIA.2021.3084552

I. INTRODUCTION

ELECTRIC machine designers endeavor to improve the torque capability with certain volume, weight, or dynamic requirements especially for transportation applications, such as electric cars, trains, drones, and airplanes. Breakthroughs on material technologies (neodymium magnets developed independently at General Motors and Sumitomo Special Metals [1], dual-phase alloy laminates developed at General Electric [2], soft magnetic composites, etc.) and implementation of advanced cooling are the main thrusts.

As the torque density requirement gets higher and higher, a natural question to ask is where is the torque limit of an ideal machine regardless of these breakthroughs and cooling approaches. This torque limit or upper bound is different from the maximum achievable or rated torque specified in a data sheet. The former one concerns and bounds infinite possibilities within the specified size and excitation conditions, whereas the latter one applies to a particular machine. Setting aside aforementioned material, thermal and mechanical advancement, a purely electromagnetic upper bound may be of multiple uses. First, without going too further in details, the machine designers may quickly narrow down the searching space according to the upper limit. Second, the ratio of the actual designed/measured

torque to the upper limit may be used as a metric of measuring the lamination material's electromagnetic capability or reversely as an indicator of the marginal gain of iron core of higher relative permeability. Last but not least, the electromagnetic scalability and the sizing law become more clear. The scalability analysis presented here revealed that the optimal remanence flux density of permanent magnets (PM) is at 1.91 T, providing that the lamination saturates at 2 T. The proposed scalability analysis may be used for guiding the development of new magnetic materials in electric-drive applications and potentially superconducting synchronous machines, where the rotor field excitation can be treated as PMs [3].

A first step toward the answer was established on round rotor wound field synchronous machines (WFSMs) and documented in [4]. This article tries to find an upper bound of surface PM (SPM) synchronous machines as a continuing effort. Clearly, infinite upper bounds exist. The closer to the maximum achievable or rated torque, the more relevant is the upper bound. Whence, it is beneficial to review methods been used to predict the torque production before giving away to computer programs for final optimization. Torque is resulted from the conversion between air gap energy and mechanical energy. Essen's rule depicts this and expresses the torque production as a function of key gap parameters including surface area, axial length, peagk gap flux density, peak surface current density, gap efficiency, and power factor [5]. Honsinger incorporated the stator back iron and developed the so-called D^3L and $D^{2.5}L$ sizing formula, where D is the stator outer diameter [6]. Recently, Lipo *et al.* made a comprehensive comparison of ac motors to an ideal machine based on Essen's rule [7], [8]. Their result shows that SPM machines equipped with neodymium magnets are nearly identical to ideal electric machines in terms of torque production. This makes the study of the upper bound of SPM machines herein more meaningful since it is also the bound of other common types of machines in industrial applications. As far as the modeling of SPM machines goes, Zhu *et al.* made a thrust on the analytical field calculation, including open-circuit field [9], armature-reaction field [10], and stator slotting effects [11]. Later, the analysis was extended to cover SPMs with parallel magnetized PMs [12]. In [13], Zarko *et al.* proposed the concept of complex relative air-gap permeance to predict not only the radial but also the tangential field components in a slotted air gap. The magnetic circuit method is also a powerful one when it comes to calculating the flux density in the back iron [14], [15].

As stated earlier, a torque production limit or upper bound in terms of the machine's major geometries and excitation conditions is to be sought out. In order to obtain this limit or upper bound, in Section II, we assume the back iron possesses infinite permeability. This lends itself to perform a field analysis in the air gap. Unlike Zhu *et al.*'s approach, the complex vector analysis from [16] is employed to obtain the on-load field for ease of deduction and making further assumptions in the scalability analysis. It is well known that the volumetric torque density of electric machines is getting better as the size goes up. Different sizing equations were derived or curve fitted to match the observation [17], [18]. Section III particularly explained

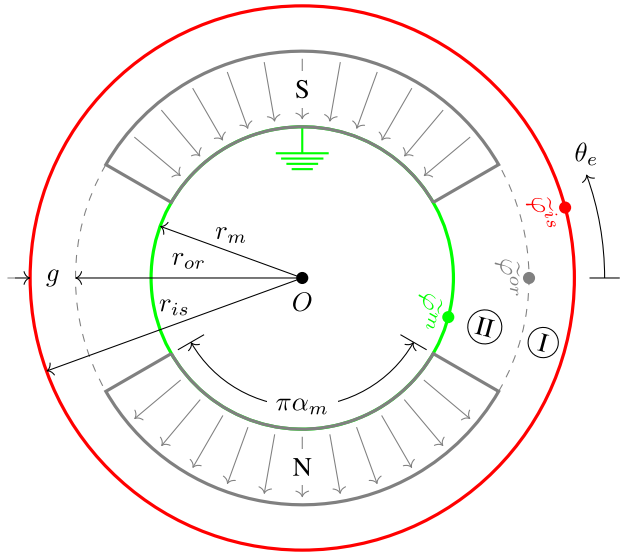

Fig. 1. SPM machine topology assuming infinite core permeability. The rotor is placed such that the machine is generating the maximum torque.

such an observation from both the volume and the shear stress perspectives using the upper bound derived in Section II, which is verified in Section IV via finite-element analysis (FEA). Correspondingly, from a broad perspective, this article made the following contributions.

1) An upper bound of the torque production of SPMs is derived for the first time and verified through FEA.
2) The scalability of the torque production of SPMs is revealed using the derived upper bound.
3) The proposed analysis may be used for guiding the development of future magnetic materials for electric-drive applications and potentially superconducting synchronous machines, where the field excitation can be regarded as PMs [3].

More detailed results are summarized in Section V. The authors, propounding the idea of looking for an upper bound in view of the increasing demand in torque density, would like to emphasize that this article and [4] merely initiate the briefest investigation.

II. Derivation of Torque Upper Bound

A. Machine Topology and Parameters

The reluctance of the stator and rotor iron cores, due to their finite permeability, consume a portion of the magnetomotive force (MMF). As the material is gradually improved over time, this portion will be less. Here, the permeability of the iron core is assumed to be infinite and, thus, all the MMF drop happen in the gap region, which leads to higher torque production than reality and constitutes the first approximation step. Correspondingly, the machine topology may be represented as in Fig. 1. The angular coordinate is drawn in electrical radian and only two poles are shown even though the machine has a generic number of pole pairs of P. The stator inner radius, rotor outer radius, and

PM inner radius are designated as $r_{\rm is}, r_{\rm or}$, and r_m and the gap length g is, therefore, $(r_{\rm is}-r_{\rm or})$. The phasor of the magnetic potential at these surfaces are denoted as $\widetilde{\varphi}^{\rm is}$, $\widetilde{\varphi}^{\rm or}$, and $\widetilde{\varphi}^{m}$. (The superscripts in the phasors indicate the location.) Specifically, $\widetilde{\varphi}^{\rm is}$ is mainly governed by the winding configuration and excitation level, $\widetilde{\varphi}^{m}$ is essentially zero because of the infinitely permeable core, $\widetilde{\varphi}^{\rm or}$ is a linear combination of $\widetilde{\varphi}^{\rm is}$ and the magnetization vector of the PMs. These PMs all have an angular span of $\pi\alpha_m$, where $\alpha_m \in (0,1)$.

B. Magnetomotive Force (MMF)

Since the back iron does not waste any ampere turns at all, the stator MMF exerts fully on the stator inner radius. Therefore

$$\widetilde{\varphi}^{\rm is} = (-1)^{\frac{h-1}{2}} \frac{3}{\pi} \frac{N_t I_{\rm sp}}{C_s P} \frac{k_{s,h}}{h}. \tag{1}$$

Notice that this also implies that the slot effect is omitted and constitutes the second approximation. Due to the relatively large gap in SPMs, the error introduced by this is small.

As to the rotor side, the MMF is provided by the PMs. We directly present the magnetization vector $\mathbf{M}$ here. It has no θ component and

$$\widetilde{M}_r = (-1)^{\frac{h+1}{2}} \frac{2jB_r\alpha_m}{\mu_0} \frac{\sin(h\pi\alpha_m/2)}{h\pi\alpha_m/2}. \tag{2}$$

With (2), one may solve the particular solution $\widetilde{\varphi}^{II,p}$ following the procedures documented in [9] by Zhu *et al.* The remaining unknown is $\widetilde{\varphi}^{\rm or}$ (recall that $\widetilde{\varphi}^{m}$ is at ground potential) and this can be solved by matching the flux density from the two sides of $r = r_{\rm or}$. We will derive the flux density in the next section.

C. Transfer Relation Between Flux Density and Field Strength

In order to simplify the deduction process, we employ the air gap transfer relation from [16]

$$\begin{bmatrix} \widetilde{B}_r^{\rm is} \\ \widetilde{B}_r^{\rm or} \end{bmatrix} = j\mu_0 \begin{bmatrix} f_{hP}(r_{\rm or}, r_{\rm is}) & g_{hP}(r_{\rm is}, r_{\rm or}) \\ g_{hP}(r_{\rm or}, r_{\rm is}) & f_{hP}(r_{\rm is}, r_{\rm or}) \end{bmatrix} \begin{bmatrix} \widetilde{H}_\theta^{\rm is} \\ \widetilde{H}_\theta^{\rm or} \end{bmatrix} \tag{3}$$

where f and g are geometric coefficients. When the air gap $g \ll r_{\rm or} \approx r_{\rm is}$, these transfer coefficients are equivalent to the hyperbolic functions $\sinh, \cosh$ used in rectangular coordinates, which are presented in an earlier work [4] for WFSMs. Similarly, in region II, we end up with a slightly complicated formula (4) shown at bottom of this page, due to the present of PMs

By equating $\widetilde{B}_r^{\rm or}$ in (3) and (4), the magnetic potential at $r = r_{\rm or}$ can be resolved as in (5) shown at bottom of this page, where the hatted version of function g_m is defined as $\widehat{g}_m(x,y) = (x/y)g_m(x,y)$.

D. Shear Stress and Torque Estimation

Since both the normal and tangential component of the magnetic field on the rotor surface are available, one may write the shear stress on the rotor surface after taking an average over circumferential direction

$$\bar{\sigma}_m = \frac{1}{2}\mu_0 g_P(r_{\rm or}, r_{\rm is}) \frac{P^2}{r_{\rm is} r_{\rm or}} \Re[j\widetilde{\varphi}^{\rm is}(\widetilde{\varphi}^{\rm or})^\star].$$

Notice that $h = 1$ is assumed here simply because it is the only field component producing a net torque. According to the definition of the θ angle and the placement of the rotor position, $\widetilde{\varphi}^{\rm is}$ is real and $\widetilde{M}_r$ is imaginary. Therefore, the last term in the aforementioned equation is reduced to $\widetilde{\varphi}^{\rm is}\Im[\widetilde{\varphi}^{\rm or}]$ and the complete equation for the maximum average shear stress is presented in (6) shown at bottom of this page. Finally, the maximum torque is obtained via simply multiplying $\bar{\sigma}_{m,\max}$ by $2\pi r_{\rm or}^2 l_e$ as shown in (7) shown at bottom of this page, where

$$\begin{bmatrix} \widetilde{B}_r^{\rm or} \\ \widetilde{B}_r^{m} \end{bmatrix} = j\mu_0\mu_{rm} \begin{bmatrix} f_{hP}(r_m, r_{\rm or}) & g_{hP}(r_{\rm or}, r_m) \\ g_{hP}(r_m, r_{\rm or}) & f_{hP}(r_{\rm or}, r_m) \end{bmatrix} \begin{bmatrix} \widetilde{H}_\theta^{\rm or} - \widetilde{H}_\theta^{or,p} \\ \widetilde{H}_\theta^{m} - \widetilde{H}_\theta^{m,p} \end{bmatrix} + \frac{1}{2}\mu_0 \widetilde{M}_r \begin{cases} \begin{bmatrix} 1 \\ \ln(er_{\rm or}/r_m) \end{bmatrix} & \text{when } hP = 1, \\ \dfrac{(hP)^2}{(hP)^2-1} \begin{bmatrix} 2 \\ 2 \end{bmatrix} & \text{when } hP \neq 1. \end{cases} \tag{4}$$

$$\widetilde{\varphi}^{\rm or} = \frac{\widehat{g}_{hP}(r_{\rm is}, r_{\rm or})\widetilde{\varphi}^{\rm is}}{\mu_{rm} f_{hP}(r_{\rm or}, r_m) + f_{hP}(r_{\rm is}, r_{\rm or})} + \frac{1}{2} r_{\rm or} \widetilde{M}_r \begin{cases} \dfrac{1}{hP} \dfrac{1 + hP \cdot g_{hP}(r_{\rm or}, r_m)\ln(r_{\rm or}/r_m)}{\mu_{rm} f_{hP}(r_{\rm or}, r_m) + f_{hP}(r_{\rm is}, r_{\rm or})} & \text{when } hP = 1, \\ \dfrac{2}{(hP)^2-1} \dfrac{hP - f_{hP}(r_{\rm or}, r_m) + g_{hP}(r_{\rm or}, r_m)}{\mu_{rm} f_{hP}(r_{\rm or}, r_m) + f_{hP}(r_{\rm is}, r_{\rm or})} & \text{when } hP \neq 1. \end{cases} \tag{5}$$

$$\bar{\sigma}_{m,\max} = \frac{\widehat{g}_P(r_{\rm is}, r_{\rm or}) B_r \alpha_m}{2 r_{\rm or}} \frac{\sin(\pi\alpha_m/2)}{\pi\alpha_m/2} \left(\frac{3}{\pi}\frac{N_t I_{\rm sp}}{C_s P} k_{s,1}\right) \begin{cases} \dfrac{P + P^2 \cdot g_P(r_{\rm or}, r_m)\ln(r_{\rm or}/r_m)}{\mu_{rm} f_P(r_{\rm or}, r_m) + f_P(r_{\rm is}, r_{\rm or})} & \text{when } P = 1, \\ \dfrac{2P^2}{P^2-1} \dfrac{P - f_P(r_{\rm or}, r_m) + g_P(r_{\rm or}, r_m)}{\mu_{rm} f_P(r_{\rm or}, r_m) + f_P(r_{\rm is}, r_{\rm or})} & \text{when } P \neq 1. \end{cases} \tag{6}$$

$$T_{e,\max} = 2 r_{\rm or} l_e \widehat{g}_P(r_{\rm is}, r_{\rm or}) B_r \sin(\pi\alpha_m/2) \left(\frac{3}{\pi}\frac{N_t I_{\rm sp}}{C_s P} k_{s,1}\right) \begin{cases} \dfrac{P + P^2 \cdot g_P(r_{\rm or}, r_m)\ln(r_{\rm or}/r_m)}{\mu_{rm} f_P(r_{\rm or}, r_m) + f_P(r_{\rm is}, r_{\rm or})} & \text{when } P = 1, \\ \dfrac{2P^2}{P^2-1} \dfrac{P - f_P(r_{\rm or}, r_m) + g_P(r_{\rm or}, r_m)}{\mu_{rm} f_P(r_{\rm or}, r_m) + f_P(r_{\rm is}, r_{\rm or})} & \text{when } P \neq 1. \end{cases} \tag{7}$$

l_e is the effective axial length of the machine. It is shown as a function of the rotor surface area ($\sim rl_e$) instead of rotor volume as in Essen's rule or the D^3L sizing equation, which is because it is written directly in terms of the excitation current $I_{\rm sp}$ instead of the linear current density, which factors in the radius.

E. Saturation Constraint

Even though an infinite permeability is assumed for the back iron, we do want to impose a saturation constraint so that the torque value just derived is bounded. There are two areas we want to impose the constraint, i.e., the back iron and PMs.

Carefully examining these transfer coefficients, one would find out that the constraint is more strict at the rotor back iron than the stator side for the following two reasons.

1) As will be seen later, the stator side excitation $\widetilde{\varphi}^{\rm is}$ in nowadays technology cannot match $\widetilde{M}_r$ generated by the NdFeB magnets.
2) The ratios $r_{\rm is}/r_{\rm or}$ and $r_{\rm or}/r_m$ determine the portion of $\widetilde{\varphi}^{\rm is}$ and $\widetilde{M}_r$ remaining at the radius of r_m and $r_{\rm is}$, respectively, after the interaction in the gap; the portion diminished in the imaginary part of $\widetilde{B}_r^{\rm is}$ is greater than the portion diminished in the real part of $\widetilde{B}_r^m$.

According to (4), the flux density at the surface $r = r_m$ can be expanded as in (8) shown at bottom of this page. Their absolute value should be no greater than the saturation level $B_{\rm sat}$. (It is easy to prove that the tangential components $\widetilde{B}_\theta$ are both zeros in the stator and rotor back iron.) Few important observations, which will be useful in the next section, may be made in the following.

1) As mentioned previously, $\widetilde{\varphi}^{\rm is}$ is real and $\widetilde{M}_r$ is imaginary. Thus, the first term in (8a) and (8b) is real and the second and third terms are imaginary.
2) Among the imaginary terms, the first one is much larger than the second one due to the fact that the air gap length is typically much smaller than the magnet thickness, and thus, the resultant relatively large value of $f_{hP}(r_{\rm is}, r_{\rm or})$ comparing to other related transfer coefficients.
3) The coefficients of $\widetilde{\varphi}^{\rm is}$ and $\widetilde{M}_r$ are almost constant functions of the harmonic order h. Hence, the total flux density field may be approximated by summing $\widetilde{\varphi}^{\rm is}$ and $\widetilde{M}_r$ over harmonic h and multiplying them by constants, respectively.
4) The two brackets in either (8a) or (8b) are close to each other by a factor of about $r_{\rm or}/r_m$.

Similarly, the flux density of at the surface $r = r_{\rm or}$ can be expanded as in (9) and (10) shown at bottom of this page. The total field should be less than the saturation level of the PMs and more importantly greater than the knee point. The observations on the equations are as follows.

1) As can be expected, the radial component dominates. One may check this by substituting some numbers in those extra coefficients $f_{hP}(r_{\rm or}, r_m)$ and $f_{hP}(r_{\rm is}, r_{\rm or})$ in (9).

$$\widetilde{B}_r^m = \frac{hP}{r_{\rm or}}\frac{\mu_0\mu_{rm}g_{hP}(r_m,r_{\rm or})\widehat{g}_{hP}(r_{\rm is},r_{\rm or})}{\mu_{rm}f_{hP}(r_{\rm or},r_m)+f_{hP}(r_{\rm is},r_{\rm or})}\widetilde{\varphi}^{\rm is} + \frac{1}{2}\mu_0\widetilde{M}_r\left[\ln\left(\frac{er_{\rm or}}{r_m}\right) + hP\cdot f_{hP}(r_{\rm or},r_m)\ln\left(\frac{r_{\rm or}}{r_m}\right)\right]$$
$$+\frac{1}{2}\mu_0\widetilde{M}_r\frac{\mu_{rm}g_{hP}(r_m,r_{\rm or})\left[1+hP\cdot g_{hP}(r_{\rm or},r_m)\ln(r_{\rm or}/r_m)\right]}{\mu_{rm}f_{hP}(r_{\rm or},r_m)+f_{hP}(r_{\rm is},r_{\rm or})} \quad \text{when } hP=1, \tag{8a}$$

$$\widetilde{B}_r^m = \frac{hP}{r_{\rm or}}\frac{\mu_0\mu_{rm}g_{hP}(r_m,r_{\rm or})\widehat{g}_{hP}(r_{\rm is},r_{\rm or})}{\mu_{rm}f_{hP}(r_{\rm or},r_m)+f_{hP}(r_{\rm is},r_{\rm or})}\widetilde{\varphi}^{\rm is} + \frac{hP}{(hP)^2-1}\mu_0\widetilde{M}_r\left[hP+g_{hP}(r_m,r_{\rm or})+f_{hP}(r_{\rm or},r_m)\right]$$
$$+\frac{hP}{(hP)^2-1}\mu_0\widetilde{M}_r\frac{\mu_{rm}g_{hP}(r_m,r_{\rm or})\left[hP-f_{hP}(r_{\rm or},r_m)+g_{hP}(r_{\rm or},r_m)\right]}{\mu_{rm}f_{hP}(r_{\rm or},r_m)+f_{hP}(r_{\rm is},r_{\rm or})} \quad \text{when } hP\neq 1, \tag{8b}$$

$$\widetilde{B}_r^{\rm or} = -\frac{hP}{r_{\rm or}}\frac{\mu_0\mu_{rm}f_{hP}(r_{\rm or},r_m)\widehat{g}_{hP}(r_{\rm is},r_{\rm or})}{\mu_{rm}f_{hP}(r_{\rm or},r_m)+f_{hP}(r_{\rm is},r_{\rm or})}\widetilde{\varphi}^{\rm is} + \frac{1}{2}\mu_0\widetilde{M}_r f_{hP}(r_{\rm is},r_{\rm or})\frac{1+hP\cdot g_{hP}(r_{\rm or},r_m)\ln(r_{\rm or}/r_m)}{\mu_{rm}f_{hP}(r_{\rm or},r_m)+f_{hP}(r_{\rm is},r_{\rm or})}$$
$$\text{when } hP=1, \tag{9a}$$

$$\widetilde{B}_r^{\rm or} = -\frac{hP}{r_{\rm or}}\frac{\mu_0\mu_{rm}f_{hP}(r_{\rm or},r_m)\widehat{g}_{hP}(r_{\rm is},r_{\rm or})}{\mu_{rm}f_{hP}(r_{\rm or},r_m)+f_{hP}(r_{\rm is},r_{\rm or})}\widetilde{\varphi}^{\rm is} + \mu_0\widetilde{M}_r f_{hP}(r_{\rm is},r_{\rm or})\frac{hP}{(hP)^2-1}\frac{hP-f_{hP}(r_{\rm or},r_m)+g_{hP}(r_{\rm or},r_m)}{\mu_{rm}f_{hP}(r_{\rm or},r_m)+f_{hP}(r_{\rm is},r_{\rm or})}$$
$$\text{when } hP\neq 1, \tag{9b}$$

$$\widetilde{B}_\theta^{or-} = -\frac{jhP}{r_{\rm or}}\frac{\mu_0\mu_{rm}\widehat{g}_{hP}(r_{\rm is},r_{\rm or})}{\mu_{rm}f_{hP}(r_{\rm or},r_m)+f_{hP}(r_{\rm is},r_{\rm or})}\widetilde{\varphi}^{\rm is} - \frac{1}{2}j\mu_0\mu_{rm}\widetilde{M}_r\frac{1+hP\cdot g_{hP}(r_{\rm or},r_m)\ln(r_{\rm or}/r_m)}{\mu_{rm}f_{hP}(r_{\rm or},r_m)+f_{hP}(r_{\rm is},r_{\rm or})}$$
$$\text{when } hP=1, \tag{10a}$$

$$\widetilde{B}_\theta^{or-} = -\frac{jhP}{r_{\rm or}}\frac{\mu_0\mu_{rm}\widehat{g}_{hP}(r_{\rm is},r_{\rm or})}{\mu_{rm}f_{hP}(r_{\rm or},r_m)+f_{hP}(r_{\rm is},r_{\rm or})}\widetilde{\varphi}^{\rm is} - j\mu_0\mu_{rm}\widetilde{M}_r\frac{hP}{(hP)^2-1}\frac{hP-f_{hP}(r_{\rm or},r_m)+g_{hP}(r_{\rm or},r_m)}{\mu_{rm}f_{hP}(r_{\rm or},r_m)+f_{hP}(r_{\rm is},r_{\rm or})}$$
$$\text{when } hP\neq 1. \tag{10b}$$

It is more significant in the imaginary part since the gap length is usually much smaller than the thickness of PMs.

2) The radial component of the flux densities at the surfaces $r = r_{\rm or}$ and $r = r_m$ are close to each other with a factor of roughly $r_m/r_{\rm or}$ between the real components and $r_{\rm or}/r_m$ between the imaginary components.

III. Discussion on Electromagnetic Scalability

As mentioned in the introduction, the content presented here is not intended for machine design directly. Equation (7) together with the saturation constraint shows that there is a theoretical limit in the torque production when the excitation and major dimensions are given. More generally, the torque production is proportional to the average shear stress and the rotor volume (which is the essence of Essen's rule). Therefore, the torque density should meet the following condition:

$$\frac{T_e}{\mathrm{V}_s + \mathrm{V}_r} < \frac{T_e}{\mathrm{V}_r} = 2\bar{\sigma}_m \tag{11}$$

where $\mathrm{V}_s, \mathrm{V}_r$ are the stator and rotor volume, respectively. The rotor volume includes the shaft while the stator volume includes everything but the rotor volume. The average shear stress $\bar{\sigma}_m$ is bounded by the saturation level of the electrical steel. Therefore, the torque output of electric machines cannot increase faster than the volume. Then, how to explain the observation aforementioned in the introduction, i.e., the volumetric torque density of electric machines get better as the size goes up? Two aspects in (11) are explained and discussed as follows.

A. Volume in Small Scope

Consider two machines of the same design with all dimensions in the ratio $k:1$ and having the same speed and flux density constraint like in [17]. According to (8), the current may scale up to k times and correspondingly the torque will be scaled by k^3 based on (7). However, one may quickly realize that the slot area is not fully used, i.e., the current density J is not kept at its original level. Nevertheless, keeping J constant would violate the flux density constraint. Indeed, Ampère's law scales in one-dimensional space while Gauss's law scales in two-dimensional space. One may quickly conclude that the current density J and the flux density B cannot be maintained at the same time under this thought experiment.

However, given sufficient cooling condition, the current density J is indeed usually kept constant within a small range of machine size, at least not decreasing as fast as the increasing size [17]. This may be understood by some design modifications. In order to keep up the current density J, one may shrink the slot size. This could be done in many ways. One way is to shrink the radial direction, but still maintain the portion of the back iron thickness for the sake of flux density constraint. Thus, the outer diameter of the second machine is shrunk. So, does the total volume, which leads to an increased torque density. Notice that this is not contradicting (11) since only V_s is reduced here.

Another aspect related to the aforementioned reasoning is the insulation thickness. Usually, for a small-scale ratio k, the voltage rating, and thus, the insulation thickness is kept the same, which allows a higher filling factor when scale up. This aspect applies as well to the large scope to be discussed in the following, since normally the voltage rating does not scale as fast as the current rating [17].

B. Shear Stress in Large Scope

The above thought experiment can be extended to a large scope when $k \gg 1$, however the average shear stress $\bar{\sigma}_m$ plays a more vital role herein. Because of the saturation constraint, we can foresee an upper bound of the shear stress. According to the inequality of arithmetic and geometric means, we may assign $B_{\rm sat}/\sqrt{2}$ to both the real and imaginary parts of $\sum_h \widetilde{B}_r^m$ (not the normal and tangential components of $\widetilde{B}^m$) to get this upper bound. Since the shear stress equation only take the fundamental component into account, two treatments are made here in the following.

1) Correcting factors are necessary to count the difference between fundamental components and the maximum total field of $\widetilde{\varphi}^{\rm is}$ and $\widetilde{M}_r$, respectively. These are $3k_{s,1}/\pi$ and $4\sin(\pi\alpha_m/2)/\pi$ (refer to Section II-E).
2) The third term in (8a) or (8b) are discarded because it is negligible comparing to the second term. The bracket in the second term is replaced with the bracket in the third term but with a correcting factor $r_{\rm or}/r_m$.

Writing them down, we have

$$\left| \frac{P}{r_{\rm or}} \frac{\mu_0 \mu_{rm} g_P(r_m, r_{\rm or}) \widehat{g}_P(r_{\rm is}, r_{\rm or})}{\mu_{rm} f_P(r_{\rm or}, r_m) + f_P(r_{\rm is}, r_{\rm or})} \widetilde{\varphi}^{\rm is} \right| = \frac{3}{\pi} k_{s,1} \frac{\sqrt{2}}{2} B_{\rm sat} \tag{12}$$

and

$$\left| \frac{1}{2} \mu_0 \widetilde{M}_r \left[1 + P \cdot g_P(r_{\rm or}, r_m) \ln(r_{\rm or}/r_m)\right] \right| = \frac{r_m}{r_{\rm or}} \frac{4\sin(\pi\alpha_m/2)}{\pi} \frac{\sqrt{2}}{2} B_{sat} \quad \text{when } P = 1 \tag{13a}$$

$$\left| \frac{P}{P^2 - 1} \mu_0 \widetilde{M}_r \left[P - f_P(r_{\rm or}, r_m) + g_P(r_{\rm or}, r_m)\right] \right| = \frac{r_m}{r_{\rm or}} \frac{4\sin(\pi\alpha_m/2)}{\pi} \frac{\sqrt{2}}{2} B_{\rm sat} \quad \text{when } P \neq 1. \tag{13b}$$

Substituting these back into the shear stress equation, we finally have

$$\bar{\sigma}_m \leq \frac{3}{\pi^2} \frac{B_{sat}^2}{\mu_0 \mu_{rm}} \frac{r_m^2}{r_{\rm or}^2} \frac{1}{\widehat{g}_P(r_{\rm or}, r_m)} k_{s,1} \sin(\pi\alpha_m/2). \tag{14}$$

For the convenience of comparison, the result of WFSMs is copied here [4] (with a correction factor $6k_{s,1}k_{r,1}/\pi^2$ added)

$$\bar{\sigma}_m \leq \frac{3}{2\pi^2} \frac{B_{\rm sat}^2}{\mu_0} \frac{1}{f_P(r_{\rm is}, r_{\rm or})} k_{s,1} k_{r,1}. \tag{15}$$

The major difference between them is the transfer coefficients. It is easy to see that $1/f_m$ is bounded while $1/\widehat{g}_m$ is not by checking the definition of f_m and $\widehat{g}_m$. Hence, had the recoil line of the PMs is linear over a wide range of H field, the shear stress of SPMs can be greater than $3B_{\rm sat}^2/2\pi^2\mu_0$, which is the limit of WFSMs [4]. To show this, the shear stress limit is plotted against

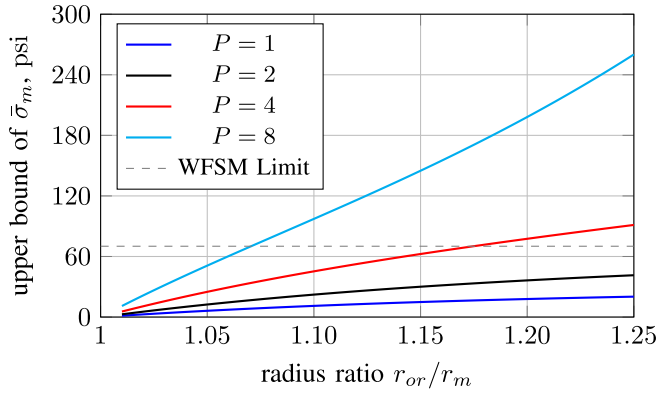

Fig. 2. Upper bound of the average shear stress as a function of the radius ratio $r_{\rm or}/r_m$ for PMs with wide recoil capability and achievable remanence flux density B_r. The settings are: $B_{\rm sat}=2\,\mathrm{T}$, $\mu_{rm}=1$, $k_{s,1}=1$, and $\alpha_m=1$.

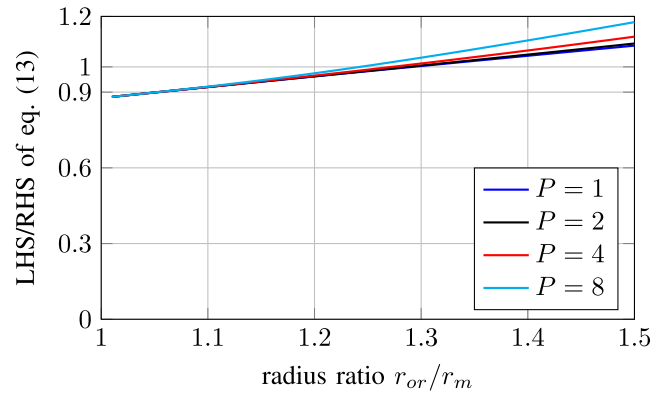

Fig. 3. Ratio of LHS and RHS of (13) as a function of the outer and inner radius of PMs. The settings are: $B_{\rm sat}=2\,\mathrm{T}$ and remanent flux density of PMs are 1.24 T.

$r_{\rm or}/r_m$, as shown in Fig. 2 , for ideal PMs that possess wide recoil capability. However, the shear stress looks appealing but is not practical with current technology. The reasons are embedded in (12) and (13).

1) The term $P\widetilde{\varphi}^{\rm is}/r_{\rm or}$ in (12) with a factor $-jr_{\rm or}/r_{\rm is}$ is actually commonly known as the linear current density or current loading $\widetilde{K}$. Therefore, the following term dictates the amount of current loading needed to satisfy (12):

$$\frac{\sqrt{2}}{2}\frac{B_{sat}}{\mu_0}\Big/\frac{\mu_{rm}g_P(r_m,r_{\rm or})g_P(r_{\rm or},r_{\rm is})}{\mu_{rm}f_P(r_{\rm or},r_m)+f_P(r_{\rm is},r_{\rm or})}\ .$$

If we substitute the machine parameters in Section IV, the absolute value of $\widetilde{K}$ is 174 $\mathrm{Arms/mm}$, which is apparently not achievable nowadays even in large size motors [17], [19].

2) Another underlying assumption in Fig. 2 is that the remanence flux density B_r can satisfy (13). The ratio of the left-hand side (LHS) and right-hand side (RHS) of (13) is plotted in Fig. 3 for high grade NdFeB magnets possessing remanence of 1.24 T. The ratio $r_{\rm or}/r_m$ has to reach to around 1.3 for (13) to be true let alone the temperature effect on B_r. However, typical value $r_{\rm or}/r_m$ is around 1.1 for modest size motors and it decreases as size goes up. Suppose that PMs contribute most of the saturation flux instead of sharing half, the optimal remanence flux density of PMs is predicted at 1.91 T in electric-drive applications.

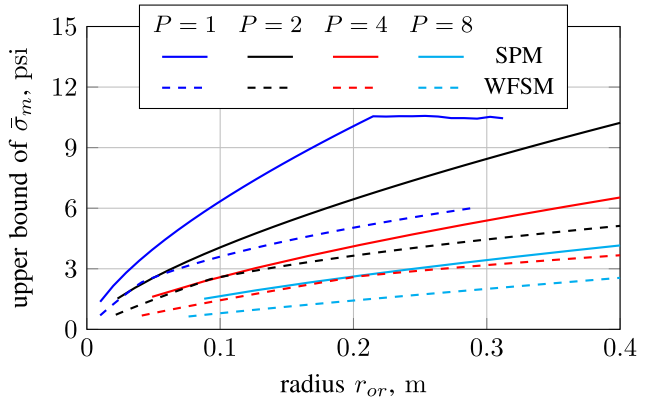

Fig. 4. Upper bound of the average shear stress as a function of the radius $r_{\rm or}$ for WFSMs and SPMs with both constraints on the current loading and saturation of the iron core. The settings are: $B_{\rm sat}=2\,\mathrm{T}$ and $B_r=1.24\,\mathrm{T}$.

For nonideal PMs, both the saturation at the iron core and the demagnetization of PMs should be considered. The shear stress scalability is a convoluted function of all the design parameters. It would be more appropriate to study this with historical data; however, some parameters are often missing in most scientific literature and technical documents. To circumvent this, following two empirically established scaling laws from Jong's book [20] are utilized.

1) The air gap of SPMs scales up roughly as induction machines according to [19]. For induction machines

$$g=9\times10^{-3}\frac{r_{\rm or}}{\sqrt{P}}\,[\mathrm{m}].$$

2) The current loading scales up as a power function of the pole-pitch:

$$|\widetilde{K}_{s,\rm rms}|=10^5\left(\frac{\pi r_{\rm is}}{P}\right)^{2/3}\,[\mathrm{A/m}].$$

The law holds with a pole pitch range of 0.03 to 1 m and this constraint will show up in the result. It should be noted that the above law together with the saturation constraint determines the actual current loading.

A brutal force search of maximum shear stress as a function of the rotor radius $r_{\rm or}$ is then carried out using these scaling laws, the saturation constraint imposed on (8), and the demagnetization threshold (0.1 T) imposed on (9). The results are shown in Figs. 4 and 5 . Overall, the upper bound of the shear stress increases when the rotor size goes up. When $P=1$, the shear stress starts to flat after $r_{\rm or}=0.2\,\mathrm{m}$ mainly due to the demagnetization constraint that limits the angular span $\pi\alpha_m$ of the PMs, which also reflects on desiring for thicker PMs in Fig. 5. Probably a more interesting result is that the magnet ratio holds constant through a wide range of radius for $P=2,4,8$, in contrast to Fig. 2 that shows higher shear stress craves thicker PMs with ideal settings. This is due to the fact that the gap ratio $r_{\rm is}/r_{\rm or}$ is a constant and the current loading is constrained.

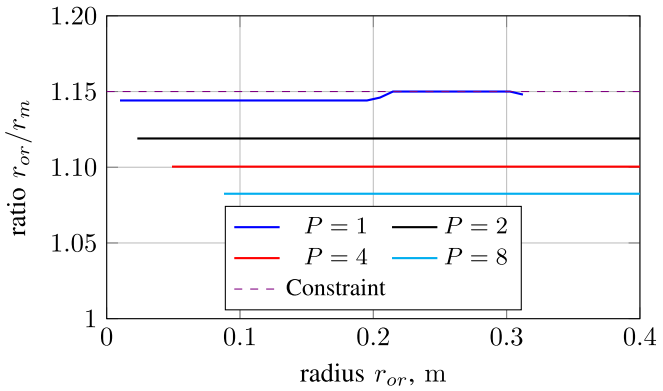

Fig. 5. Ratio of PMs' outer and inner radius as a function of the radius r_{or} with the same settings as Fig. 4. A limit 1.15 is set in the searching program.

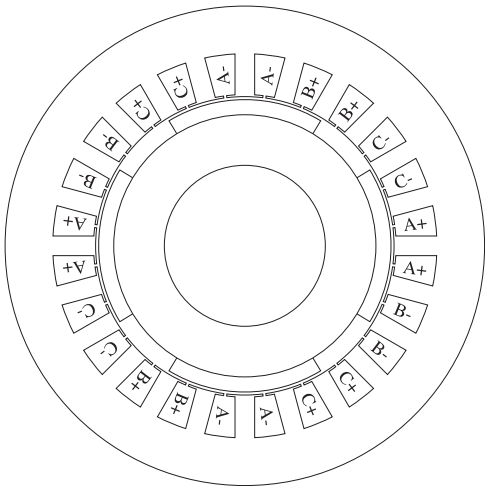

Fig. 6. Cross-sectional view of the selected SPM model.

IV. Experimental Verification via FEA and Historical Data

Since the presented theoretical work is done with the assumption of infinite permeable iron core, which is not attainable in reality, the correctness of the derived field distribution and upper bound equations are verified via FEA and prototypes together.

1) The permeability of the core material can be gradually increased to approach infinity in FEA in order to validate the assumption of infinite permeable iron core. An SPM model is selected for this purpose and is shown in Fig. 6. Two aspects of the theoretical work, i.e., the full-field reconstruction via superposition of each individual harmonic contents and the correctness of the torque upper bound, are validated in Sections IV-A and IV-B, respectively. All the necessary parameters to reproduce the results presented in Sections IV-A and IV-B are listed in Table I.
2) The derived upper bound is also verified over a wide power range in Section IV-C via FEA. A commonly used core material M270-35 A (also known as M19) rather than an ideal core is assumed.

TABLE I
Key Parameters of the Simulated SPM Used in Sections IV-A and IV-B

Name	Value	Unit	Name	Value	Unit
Gap length	1.0	mm	Pole pairs	2	
Stator OD	158.6	mm	Rotor ID	53.25	mm
Stator ID	98.72	mm	Rotor OD	96.72	mm
Stator slot #	24		Magnet ID	86.72	mm
Teeth width	6.5	mm	α_m	0.6944	
Slot width	1.0	mm	B_r	1.2	T
Slot depth	13.5	mm	Stator back iron thickness	15.76	mm
Stack length	75	mm			

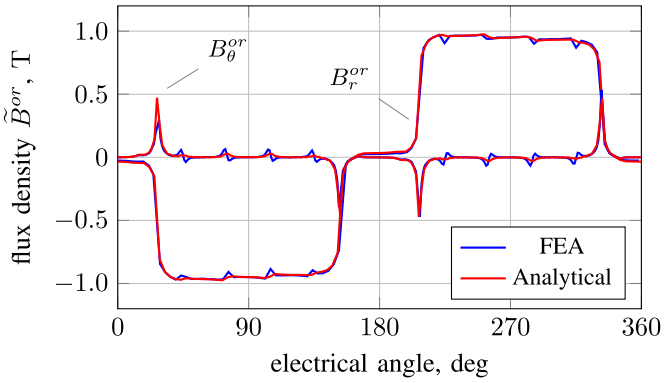

Fig. 7. Radial and tangential components of flux density at the radius $r = r_{\text{or}+}$ as a function of the electrical angle. The relative permeability of the iron core is set to 10^6 in the FEA and the harmonic content is counted up to 301 in the analytical model. The rotor angle is fixed at zero.

3) We also conducted a verification study on historical SPM machines prototyped by previous researchers instead of our own in Section IV-D. This is mainly because of the following three considerations.
   1) The presented work mainly focuses on the torque producing capability of SPM machines rather than a design methodology.
   2) Historical SPM machines cover a wide range of power levels and design configurations.
   3) Had we spent time and funding in manufacturing these prototypes, the prototypes would be same as or similar to the historical SPM machines.

A. Full Field Reconstruction

Equations (1) to (5) and (8) to (10) are all written with an explicit or implicit harmonic order h. In order to get the complete field distribution, one has to add all the harmonics up. Special care should be taken since harmonics $h = 5, 11, \ldots$ in $\widetilde{\varphi}^{\text{is}}$ rotate backward while the same orders in $\widetilde{M}_r$ rotate forward.

The flux density at the rotor surface $r = r_{\text{or}+}$ is reconstructed here and plotted against FEA in Fig. 7. Because of the nearly unity relative permeability of the PMs, the field distribution in the tangential direction is identical to the ones at $r = r_{\text{or}-}$. The major discrepancies show up at where the slot openings are. Had the slot effect been corrected using relative air gap permeance [11], [13], the agreement between the FEA and the

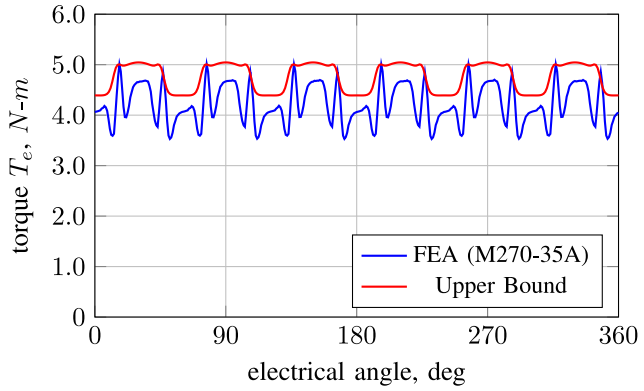

Fig. 8. Torque as a function of the rotor position. Each coil is excited with 100 A − t pk.

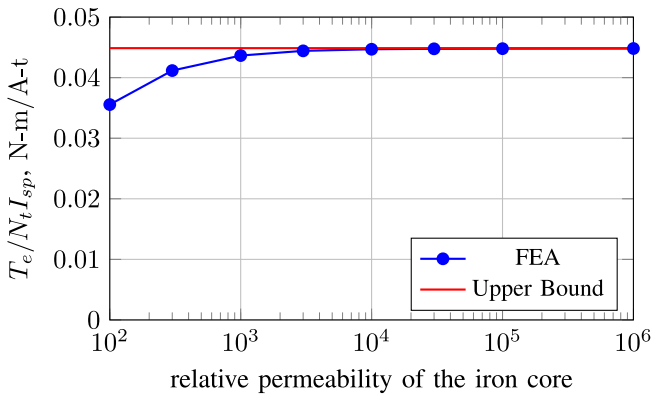

Fig. 9. Torque production as a function of the relative permeability of the iron core. Here the relative permeability is an effective one counting all of the MMF drop in the iron.

analytical model would be even better, which, however, is out of the scope of this article.

B. Torque Upper Bound

Previously, a torque upper bound for SPMs is derived with the key assumption of an infinite permeability of the iron core. Therefore, it is paramount to verify (7) against this basic assumption. Figs. 8 and 9 show obtained and justify the assumption well. Specifically, Fig. 8 shows that the upper bound is well above the actual case using M270-35 A laminations. In Fig. 9, when the relative permeability of the iron core is greater than 1000, the discrepancy between the two models is within 3%. Moreover, the error is approaching zero as the iron core is becoming less reluctant. It should be noted that the y-axis of Fig. 9 uses $T_e/N_tI_{\rm sp}$ instead of T_e directly. In the FEA, one has to reduce the ampere-turns as the relative permeability is increased in order to not saturate certain area of the core within the same design.

Comparing to the result presented in [4] for WFSMs, one may see the upper bound is tighter for SPMs. The reason is that in SPMs the effective air gap length is not affected by the slot opening width much. If Carter's coefficient was applied to

TABLE II
KEY PARAMETERS OF THE SPM MACHINES GENERATED FROM JMAG-EXPRESS

Power	Stator OD	Slot/Pole	# of Turns	Gap Thickness
0.1 kW	25.37 mm	12/4	17	0.12 mm
0.3 kW	36.59 mm	12/4	14	0.18 mm
1 kW	54.65 mm	12/4	11	0.285 mm
3 kW	78.82 mm	12/4	10	0.4 mm
9 kW	113.7 mm	24/4	8	0.59 mm
10 kW	117.7 mm	24/4	8	0.575 mm
12 kW	125.1 mm	24/4	8	0.605 mm
30 kW	169.8 mm	36/6	5	0.855 mm
100 kW	253.7 mm	48/8	3	1.2 mm
300 kW	365.9 mm	60/10	2	1.8 mm
1000 kW	546.5 mm	84/14	1	3.45 mm

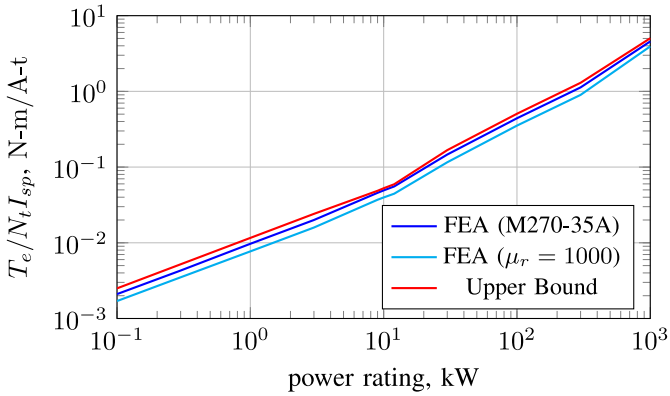

Fig. 10. Comparison of the upper bound with the actual torque production from 0.1kW to 1 MW assuming the lamination material M270-35 A is used.

WFSMs, similar degree of agreement would be reached. To this end, plots like Fig. 9 may be used as an indication of whether or not higher relative permeability is worth pursuing.

C. Benchmark With Nonideal Iron and a Wide Power Range

In this case study, M270-35 A laminations instead of a linear material as in Section IV-B is assumed. Besides, to circumvent the difficulty of getting historical data, we deploy the JMAG-Express tool (available online [21]) to generate a family of SPM machines spanning a wide power range, which are then fed into FEA to incorporate M270-35 A's behavior and get more accurate torque values. Table II lists the obtained key parameters. Without any further modification, the tool generates unity aspect ratios, i.e., the stack length equals the stator OD.

Fig. 10 plots the actual torque production obtained from FEA using both M270-35 A and a linear material with $\mu_r = 1000$ and the upper bound predicted by (7) against a wide power range. It can be observed that machines using M270-35 A generate torque well between the upper bound and the one using the linear material. Combining with Fig. 9, one may conclude that the effective relative permeability is greater than 1000 with these excitations. The relative error between FEA (using M270-35 A) and the upper bound starts around 20 % and gradually decreases to 10 % as the power rating gets higher. Knowing that these machines are generated from JMAG-Express and not optimized,

TABLE III
UPPER BOUND AGAINST ACHIEVABLE TORQUE FOR ELECTRIC MACHINES FROM LITERATURE

Power Level	Measured Torque	Torque Upper Bound	Reference
50 W	0.13 N-m	0.16 N-m	[22], [23]
6.2 kW	65 N-m	68.8 N-m	[24]
39 kW	2.45 kN-m	2.96 kN-m	[25]

The ones from [22], [23], and [24] used fractional slot windings and the one from [25] has an external-rotor topology.

we can expect the relative error to be less when the upper bound is benchmarked against well designed machines as in Sections IV-A and IV-B.

D. Verification Against Historical Data

As mentioned at the beginning of this section, the upper bound presented here is a theoretical limit. Its basic assumption of infinite permeable core is not achievable in prototypes. Nonetheless, we can still check it against achievable torque. Table III documents, such an effort covering, a wide power range and shows that the upper bound is, indeed, above the achievable torque. Depending on the optimization strategy, the discrepancy (between measured and the upper bound) due to relaxation can be as small as 5.8% in [24]. It is worth noting that the two smaller machines used fractional slot windings [22]–[24] and the biggest one employed an external-rotor topology [25], indicating that the presented upper bound applies *not only* to regular multiphase windings, whose MMF can be explicitly described by (1), and the internal-rotor topology, where $r_{\rm is} > r_{\rm or} > r_m$ shall hold.

V. CONCLUSION

An upper bound of the torque production of SPMs with radially magnetized PMs is derived. It is written in terms of excitation $k_{s,1}N_sI_{\rm sp}, B_r\sin(\pi\alpha_m/2)$, key dimensions $r_m, r_{\rm or}, r_{\rm is}, l_e$, and pole pairs P. The result is verified via FEA against the basic assumption and via historical data against benchmarked torque in a wide power range. The ratio of the actual value and this upper bound may be used as a metric of measuring the usage of materials' electromagnetic capability, or reversely as an indicator of the marginal gain of iron core of higher relative permeability. The electromagnetic scalability of SPMs is also discussed and the following items are revealed.

1) An affine transformation with a simple reduction on the slot area, and thus, the stator outer diameter can improve the torque density by reducing the stator volume.
2) Unlike WFSMs, the average shear stress of SPMs is not bounded by $3B_{\rm sat}^2/2\pi^2\mu_0$, although, with nowadays technology, this limit of WFSMs is still far ahead for SPMs. Nevertheless, the shear stress scales up with radius.

These together explain why the torque density of SPM machines gets better as size goes up. In addition, the following statements hold.

1) The optimal remanence flux density of PMs is predicted at 1.91 T, given that the lamination saturates at 2 T. The proposed scalability analysis may be used for guiding the development of new magnetic materials in electric-drive applications and potentially superconducting synchronous machines, where the rotor field excitation can be treated as PMs [3].
2) Higher shear stress covets thicker PMs with ideal settings that PMs have wide recoil capability and current loading is unlimited. High pole count is also preferred.
3) With nonideal PMs and thermally constrained current loading, shear stress can still grow with increasing rotor OD and the optimal thickness of PMs is nearly linear with the rotor size. Low pole count is desired; however, demagnetization effects and manufacturing difficulties counterbalance such eagerness.

REFERENCES

[1] J. Lucas, P. Lucas, T. L. Mercier, A. Rollat, and W. G. Davenport, *Rare Earths: Science, Technology, Production and Use*. Amsterdam, The Netherlands: Elsevier, Sep. 2014.
[2] L. C. Dial, R. DiDomizio, and F. Johnson, "Dual phase magnetic material component and method of forming," U.S. Patent US9 634 549B2, Apr. 2017.
[3] A. Patel, A. Baskys, S. C. Hopkins, V. Kalitka, A. Molodyk, and B. A. Glowacki, "Pulsed-field magnetization of superconducting tape stacks for motor applications," *IEEE Trans. Appl. Supercond.*, vol. 25, no. 3, pp. 1–5, Jun. 2015.
[4] B. Ge, "An upper bound of the torque production for round rotor wound field synchronous machines and its electromagnetic scalability," in *Proc. IEEE Energy Convers. Congr. Expo.*, Sep. 2019, pp. 3096–3102.
[5] W. B. Esson, "Notes on the design of multipolar dynamos," *J. Inst. Elect. Eng.*, vol. 20, no. 93, pp. 265–289, May 1891.
[6] V. B. Honsinger, "Sizing equations for electrical machinery," *IEEE Trans. Energy Convers.*, vol. EC-2, no. 1, pp. 116–121, Mar. 1987.
[7] T. A. Lipo and W. Liu, "Comparison of AC motors to an ideal machine. Part I," *IEEE Trans. Ind. Appl.*, vol. 56, no. 2, pp. 1346–1355, Mar. 2020.
[8] T. A. Lipo, W. Liu, and Z. Du, "Comparison of AC motors to an ideal machine. Part II—Non-sinusoidal AC machines," in *Proc. IEEE Int. Elect. Mach. Drives Conf.*, May 2019, pp. 1810–1817.
[9] Z. Zhu, D. Howe, E. Bolte, and B. Ackermann, "Instantaneous magnetic field distribution in brushless permanent magnet DC motors. I. Open-circuit field," *IEEE Trans. Magn.*, vol. 29, no. 1, pp. 124–135, Jan. 1993.
[10] Z. Zhu and D. Howe, "Instantaneous magnetic field distribution in brushless permanent magnet DC motors. II. Armature-reaction field," *IEEE Trans. Magn.*, vol. 29, no. 1, pp. 136–142, Jan. 1993.
[11] Z. Zhu and D. Howe, "Instantaneous magnetic field distribution in brushless permanent magnet DC motors. III. Effect of stator slotting," *IEEE Trans. Magn.*, vol. 29, no. 1, pp. 143–151, Jan. 1993.
[12] Z. Zhu, D. Howe, and C. Chan, "Improved analytical model for predicting the magnetic field distribution in brushless permanent-magnet machines," *IEEE Trans. Magn.*, vol. 38, no. 1, pp. 229–238, Jan. 2002.
[13] D. Zarko, D. Ban, and T. A. Lipo, "Analytical calculation of magnetic field distribution in the slotted air gap of a surface permanent-magnet motor using complex relative air-gap permeance," *IEEE Trans. Magn.*, vol. 42, no. 7, pp. 1828–1837, Jul. 2006.
[14] J. Kim, S. Joo, S. Hahn, J. Hong, D. Kang, and D. Koo, "Static characteristics of linear BLDC motor using equivalent magnetic circuit and finite element method," *IEEE Trans. Magn.*, vol. 40, no. 2, pp. 742–745, Mar. 2004.
[15] J. R. Hendershot and T. J. E. Miller, *Design of Brushless Permanent-Magnet Machines*, Venice, FL, USA: Motor Design Books 2010.
[16] J. R. Melcher, *Continuum Electromechanics*, *1st ed.*Cambridge, MA, USA: MIT Press, Jun. 1981.
[17] T. A. Lipo, Introduction to AC Machine Design, *2nd ed.*Madison, WI, USA: Univ. Wisconsin-Madison, Aug. 2007.
[18] K. J. Binns and D. W. Shimmin, "Relationship between rated torque and size of permanent magnet machines," *Proc. Inst. Elect. Eng.—Elect. Power Appl.*, vol. 143, no. 6, pp. 417–422, Nov. 1996.
[19] J. Pyrhonen, T. Jokinen, and V. Hrabovcova, *Design of Rotating Electrical Machines*, *1st ed.* Hoboken, NJ, USA: Wiley, Feb. 2009.
[20] H. C. J. deJong, *AC Motor Design: Rotating Magnetic Fields in a Changing Environment*, *1st ed.* London, U.K.: Springer, Feb. 1989.

[21] " JMAG-Express Online [*Free Software*]." Accessed: Jul. 19, 2020. [Online]. Available: https:/www.jmag-international.com/express/
[22] S.-C. Yang, T. Suzuki, R. D. Lorenz, and T. M. Jahns, "Surface-permanent-magnet synchronous machine design for saliency-tracking self-sensing position estimation at zero and low speeds," *IEEE Trans. Ind. Appl.*, vol. 47, no. 5, pp. 2103–2116, Sep. 2011.
[23] A. N. Ghule, "Online parameter estimation for surface permanent magnet machines," Ph.D. dissertation, department of mechanical engineering, Univ. Wisconsin-Madison, Madison, WI, USA, 2013.
[24] A. M. El-Refaie, "High speed operation of permanent magnet machines," Ph.D. dissertation, department of electrical and computer engineering, Univ. Wisconsin-Madison, Madison, WI, USA, 2005.
[25] C. Ruschetti, C. Verucchi, G. Bossio, G. García, and M. Meira, "Design of a wind turbine generator for rural applications," *IET Elect. Power Appl.*, vol. 13, no. 3, pp. 379–384, 2019.

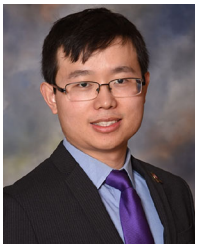

Baoyun Ge (Member, IEEE) received the B.S. degree in electrical engineering from Southeast University, Nanjing, China, in 2012, and the Ph.D. degree in electrical engineering from the University of Wisconsin-Madison, Madison, WI, USA, with the Wisconsin Electric Machines and Power Electronics Consortium, in 2018.

He is currently with C-Motive Technologies, Inc., Middleton, WI, a start-up company developing capacitively coupled power conversion technologies. His research interests include electric machines, power electronics, and high-performance electromagnetic computation.

Dr. Ge was the recipient of the First Place Paper Award and Third Place Thesis Award from IEEE Industry Application Society in 2017 and 2019, respectively.

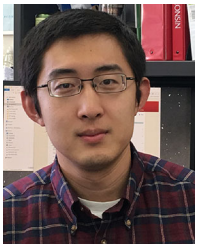

Mingda Liu (Member, IEEE) received the B.S. and Engineering degrees in electrical engineering from the National Institute of Applied Sciences of Lyon (INSA-Lyon), Lyon, France, in 2015, and the M.S. and Ph.D. degrees in electrical engineering from the University of Wisconsin-Madison, Madison, WI, USA, in 2017 and 2020, respectively.

He was a Research Assistant at the Wisconsin Electric Machines and Power Electronics Consortium, Madison. He is currently an Application Engineer with Carpenter Technology Corporation. His research interest includes the electromagnetic and thermal design of electric machines.

Jianning Dong (Member, IEEE) received the B.S. and Ph.D. degrees in electrical engineering from Southeast University, Nanjing, China, in 2010 and 2015, respectively.

He was a Postdoc Research Fellow with McMaster Automotive Resource Centre (MARC), McMaster University, Hamilton, ON, Canada. He is currently an Assistant Professor with the Delft University of Technology, Delft, The Netherlands. His main research interests include design, modeling, and control of electromechanical systems.

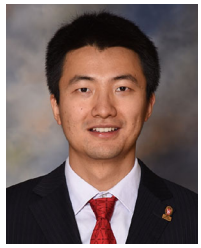

Wenbo Liu (Member, IEEE) received the B.S. degree in electrical and electronics engineering from Xi'an Jiaotong University, Xi'an, China, in 2012, and the Ph.D. degree in electrical engineering from the University of Wisconsin-Madison, Madison, WI, USA, with the Wisconsin Electric Machines and Power Electronics Consortium, in 2019.

He is currently a Research Engineer with Ford Research and Advance Engineering. His research interests include electrical machine design and control for high power density applications.